

Wake Structure and Performance of Finite Aspect-Ratio Flapping Foils

H. Dong^{*}, R. Mittal[†], M. Bozkurtas[‡]
*Department of Mechanical & Aerospace Engineering,
The George Washington University,
Washington, DC 20052*

F. Najjar[§]
*Center for Simulation of Advanced Rockets
University of Illinois at Urbana-Champaign
Urbana, IL 61801*

Most wings and fins found in nature tend to be of low or moderate aspect-ratio. However, most experimental and numerical studies in this area of bio-hydrodynamics have focused on examining large or infinite aspect-ratio flapping foils. In the current study, an efficient, finite-difference based immersed boundary solver for computing flows with moving immersed boundaries has been developed to explore the wake structures and hydrodynamic performance of finite aspect-ratio flapping foils. The results of these numerical simulations indicate that the wake topology of these relatively low aspect-ratio foils is significantly different from that observed for infinite/large aspect-ratio foils. The simulations also allow us to investigate the effect of the foil aspect-ratio, Strouhal number, Reynolds number, and pitch-bias on the wake topology and foil performance.

I. Introduction

THERE is currently an ongoing effort to develop an artificial-muscle pectoral fin for a bio-robotic autonomous underwater vehicle (BAUV) ^[1] that can match the maneuvering performance and the stealth characteristics of marine mammals systems and fish (Figure 1). As a part of this effort, computational fluid dynamics (CFD) is being used to examine the fundamental fluid physics and explore the design space of such fins. However, simulating such flows is a difficult proposition. Typical Reynolds numbers for a small fish are between $O(10^4)$ and $O(10^5)$. So the flow can be laminar, transitional or turbulent or a combination of all three. In addition, the surrounding flow environment can be steady or unsteady. The fins of fish are also highly flexible, have complex planforms and undergo complicated motions. The presence of moving and flexible control surfaces and/or the unsteady flow environment leads to flows where dominance of unsteady flow mechanisms (added mass effects, dynamic stall, vortex shedding, vortex pairing, vortex-body and vortex-fin interactions) is a rule rather than an exception.



Figure 1. Sunfish with pectoral fin highlighted. Picture courtesy of G. V. Lauder.

Until about a decade ago, it was not feasible to simulate such flows with all of their attendant complexities. However, the rapid increase in computing power and the availability of sophisticated simulation approaches has now brought these simulations within the realm of possibility. In recent years, a number of groups have employed numerical simulations to investigate the hydrodynamics of flapping foils. Chief among these are the groups at the U.S. Naval Postgraduate School ^[2,3], and NRL (Ramamurti & Coworkers) ^[4]. Both groups have employed Euler as well as RANS codes for analysis of flapping foils.

In the current study, we describe a sequence of numerical simulations that explore the wake structures and the hydrodynamic performance of finite aspect-ratio flapping foils undergoing a combined pitch-and-heave motion. Selection of an appropriate planform for the foil also requires an understanding of the foil aspect-ratio effects as well

^{*} Research Scientist, AIAA Member.

[†] Associate Professor, AIAA Senior Member.

[‡] Graduate Student, AIAA Student Member.

[§] Research Scientist, AIAA Senior Member.

as the Strouhal number, Reynolds number, and pitch-bias effects on the foil performance and this is another goal of the current study. Finally, from a fundamental point-of-view, it would be useful to analyze the wake dynamics for relatively low aspect-ratio foils *vis-a-vis* what is known regarding 2D flapping foils^[5, 6]. This issue is also addressed in the current paper.

II. Governing Equation and Numerical Method

The equations solved are the incompressible Navier-Stokes equations, written in indicial form as

$$\frac{\partial u_i}{\partial x_i} = 0; \quad \frac{\partial u_i}{\partial t} + \frac{\partial u_i u_j}{\partial x_j} = -\frac{\partial p}{\partial x_i} + \frac{1}{Re} \frac{\partial^2 u_i}{\partial x_j \partial x_j} \quad \text{Eq. (1)}$$

where the indices, $i = 1, 2, 3$, represent the x , y and z directions, respectively; while the velocity components are denoted by u (u_1), v (u_2) and w (u_3), respectively. The equations are nondimensionalized with the appropriate length and velocity scales where Re represents the Reynolds number.

A finite-difference based Cartesian grid immersed boundary solver^[7] has been developed which allows us to simulate flows with complex immersed 3-D moving bodies. The key feature of this method is that simulations with complex boundaries can be carried out on stationary non-body conformal Cartesian grids and this eliminates the need for complicated re-meshing algorithms that are usually employed with conventional Lagrangian body-conformal methods. The Eulerian form of the Navier-Stokes equations is discretized on a Cartesian mesh and boundary conditions on the immersed boundary are imposed through a “ghost-cell” procedure^[8, 9]. The method also employs a second-order center-difference scheme in space and a second-order accurate fractional-step method for time advancement. The pressure Poisson equation is solved using the semi-coarsening multi-grid method with immersed-boundary methodology. The details of this method and validation of the code can be found in [10].

III. Results

In this section, a sequence of numerical simulations that explore the wake structures and the hydrodynamic performance of finite aspect-ratio flapping foils undergoing a combined pitch-and-heave motion are presented. Foil configuration and modeling approach is discussed first. Following this, the wake topology of the flapping foils as well as aspect-ratio, Strouhal number, Reynolds number and pitch-bias angle effects on the foil performance are examined.

A. Foil Configuration and Modeling Approach

The motion of a foil undergoing combined pitch-and-heave can be prescribed as follows:

$$h = h_1 \sin(2\pi f t);$$

$$\alpha = \alpha_o + \alpha_1 \sin(2\pi f t + \phi)$$

where h_1 is the heave amplitude, α_o is the pitch-bias angle and α_1 is the amplitude of the sinusoidal pitch angle variation. Furthermore, f is the flapping frequency and ϕ is the phase difference between the pitch and plunge motions. In addition to α_o , α_1 and ϕ , the non-dimensional parameters that govern the fluid dynamics of this configuration are the normalized plunge amplitude $h_1^* = h_1 / c$, the Reynolds number $Re_\infty = U_\infty c / \nu$ (where U_∞ is the freestream velocity, c is the foil chord and ν is the kinematic fluid viscosity) and the Strouhal number $St = 2h_1 f / U_\infty$ based on the wake width^[6].

In this paper, we employ foils which are ellipsoidal in shape wherein the geometry of the foil is specified in terms of the three major-axes (a_x , a_y , a_z) where a_x , a_y , and a_z are the foil chord (c), thickness and

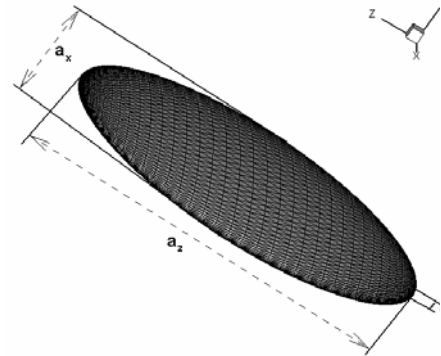


Figure 2. An ellipsoidal foil defined in terms of a surface mesh with triangular elements.

span (s) respectively. The aspect-ratio of these foils is given by $AR = \frac{4}{\pi} (a_z / a_x)$. The geometries of the immersed boundary are represented by surface mesh with triangular elements as shown in Figure 2.

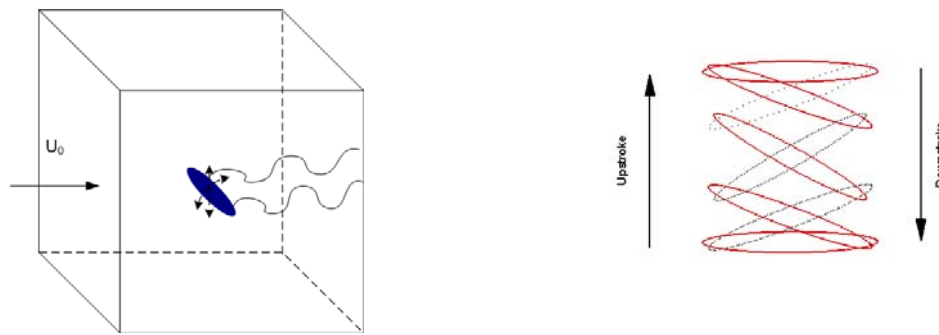
B. Flapping Foils

Fish pectoral fins tend to be of low aspect-ratio with typical values of about 2.0^[11, 12] and it is expected that the artificial pectoral fin will also be of a similar aspect-ratio. Despite this preponderance of low aspect-ratio fins in the nature, most of the theoretical, computational and experimental work has been carried out for infinite span (2D) foils. Some recent studies^[13, 14], have examined the performance of realistic low aspect-ratio foils but it is fair to say that no systematic effort has yet been made to examine the effect of aspect-ratio on the foils performance. Such knowledge would obviously be crucial in designing/sizing a bio-mimetic pectoral fin. Furthermore, from a fundamental point-of-view, it is of interest to examine the vortex dynamics and wake topology associated with low aspect-ratio flapping foils *vis-a-vis* corresponding infinite aspect-ratio foils. To this end, we have conducted a set of simulations of flapping foils to examine the foil aspect-ratio, Strouhal number, Reynolds number, and pitch-bias effects on the foil performance as well as the vortex topology of the wake.

1. Simulation Setup

Detailed validation of the code can be found in [10]. For this particular simulation of flapping foil undergoing pitching-and-heaving motion, comprehensive grid and domain size independence studies have also been conducted. Based on these studies, a domain size of $15 \times 15 \times 16$ and a $145 \times 129 \times 101$ grid has been chosen for all 3-D simulations.

The flapping foil undergoing combined pitch-and-heave motion is located in the middle of the computational domain. The heave amplitude, h_1 , is fixed at a value of 0.5 and the pitching amplitude, α_1 , is 30° in the current set of simulations. Figure 3 shows the schematic of this 3-D simulation and the motion of the flapping foil. Four different foils have been chosen for this study: a circular plan-form foil with major axes (1.0, 0.12, 1.0) and $AR = 1.27$, an elliptical foil with major-axes (1.0, 0.12, 2.0) and $AR = 2.55$, an elliptical foil with major-axes (1.0, 0.12, 4.0) and



a) Schematic of flapping foil simulations b) Motion of a pitching-and-heaving foil
Figure 3. Schematic of flapping foil simulations and the motions of a pitching-and-heaving foil

Table 1. Summary of Computational Cases.

Strouhal # Aspect Ratio	0.3	0.4	0.5	0.6	0.7	0.8	1.0	1.2
1.27	Drag Producing	Drag Producing	✓	✓	✓	✓	✓	✓
2.55	Drag Producing	✓	✓	✓	✓	✓	✓	✓
5.09	✓	✓	✓	✓	✓	✓	✓	✓
∞ (2D case)	✓	✓	✓	✓	✓	✓	✓	✓

$AR = 5.09$ and finally a 12% thick 2-D elliptic foil, whose aspect-ratio is infinity. Reynolds number of 200 is chosen for most simulations and the Strouhal number varies from 0.3 to 1.2. Table 1 shows the summary of selected the computational cases in this paper. Most cases are thrust-producing as indicated in the table above. Detailed results and analysis will be presented in the following sections.

2. Simulation Results

The typical wake topologies of a thrust-producing finite aspect-ratio flapping foil undergoing are shown in Figure 4 below. The isosurfaces of the eigenvalue imaginary part of the velocity gradient tensor $\frac{\partial u_i}{\partial x_j}$ are plotted ^[15]

in order to clearly show the vortex topology. The figure shows the 3-D view and top view of the vortex topology for a relatively low aspect ratio flapping foil. The key feature observed here is the presence of two sets of interconnected vortex loops that slowly convert into vortex rings as they convect downstream. The structure is qualitatively similar to that observed in the experiments of Ellenrieder et al ^[16]. It should be noted that Drucker & Lauder ^[11] have also observed the formation of vortex rings from the low aspect-ratio pectoral fin of a Bluegill sunfish. As will be shown in later sections, the precise vortex topology strongly depends on the aspect-ratio.

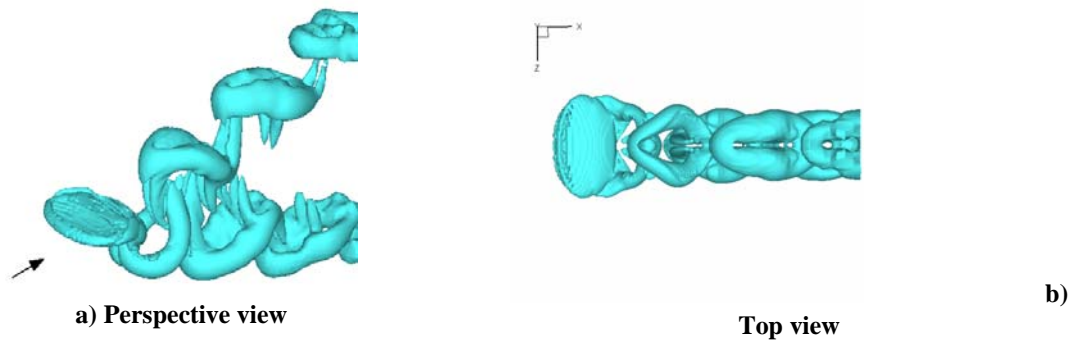


Figure 4. Typical wake structures of thrust-producing flapping foils. The arrow indicates the direction of the freestream. These plots correspond to $St=0.6$ and $AR=2.55$.

3. Aspect-ratio (AR), Strouhal Number (St), Reynolds Number (Re), and Pitch-bias Effects

The objective in the rest of the paper is to examine the effect of foil aspect-ratio, Strouhal number, Reynolds number, and pitch-bias on the vortex topology of the wake as well as the foil performance. In the first set of simulations, the Strouhal number and Reynolds number are fixed at 0.6 and 200 respectively and we examine the flow and foil performance for aspect-ratio (AR) of 1.27, 2.55, 5.09, and infinity, which is the 2-D case. All these case are thrust-producing cases.

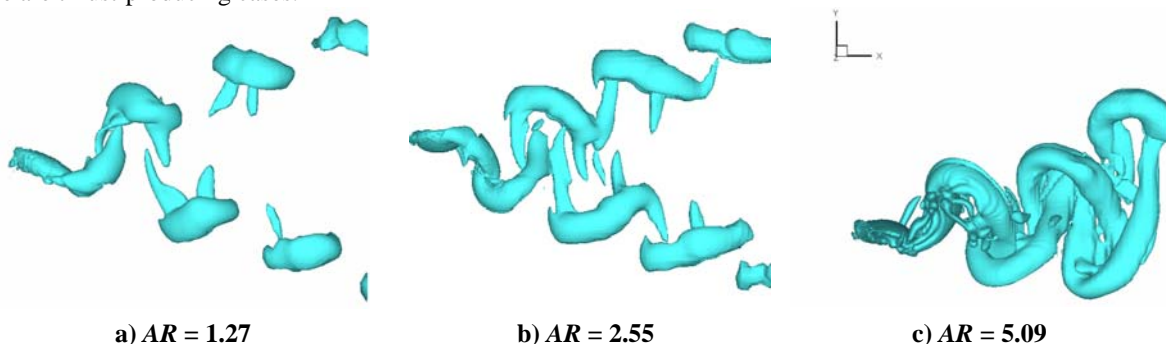


Figure 5. Side-view of wake structures of thrust-producing flapping foils with different aspect-ratios. $St = 0.6$.

Figure 5 shows the comparisons of side-view of the wake structures at $St = 0.6$ for different aspect ratios of 3-D cases. Two distinct sets of vortex rings can be observed for the low aspect-ratio foils and these convect at oblique

angles to the wake centerline. As the aspect-ratio increases, the oblique angle decreases and the two sets of rings/loops become more closely connected and even start to merge towards the center of the wake. This phenomenon can also be observed by looking at spanwise vorticity contours on the spanwise symmetry plane (Figure 6) of these three 3-D cases as well as the 2-D case ($AR = \infty$). The red-color vortices are rotating counter-clockwise, whereas the blue-color vortices are rotating clockwise. For the low aspect-ratio cases we see in essence the presence of two oblique inverse Karman vortex streets. Figure 7 shows the time-averaged streamwise velocity contours for these cases. For the low-aspect ratio foils two oblique jets are observed. As the aspect ratio increases, these jets begin to merge with each other. For the 2D foil, this merger is complete and we see a single high velocity jet created along the wake centerline. Since the streamwise momentum of this jet is directly proportional to the thrust produced by the foil, the current simulations clearly show the connection between aspect-ratio and thrust performance. Subsequent studies will directly assess the impact of aspect-ratio on the thrust production.

Figure 8 shows the comparisons of mean thrust coefficients and propulsive efficiency changing with Strouhal numbers for different aspect-ratio foils undergoing pitch-and-heave motion. Here, mean thrust coefficient is defined as $C_T = F_x / \frac{1}{2} \rho U^2 A_{plan}$ and propulsive efficiency, the ratio of average thrust force and average input power per cycle, is defined as:

$$\eta_p = \frac{U \int_0^T F_x(t) dt}{\int_0^T F_y(t) \frac{dh(t)}{dt} dt + \int_0^T M_z(t) \frac{d\theta(t)}{dt} dt}$$

where F_x is the thrust component, F_y is the lift component, and M_z is the pitching moment.

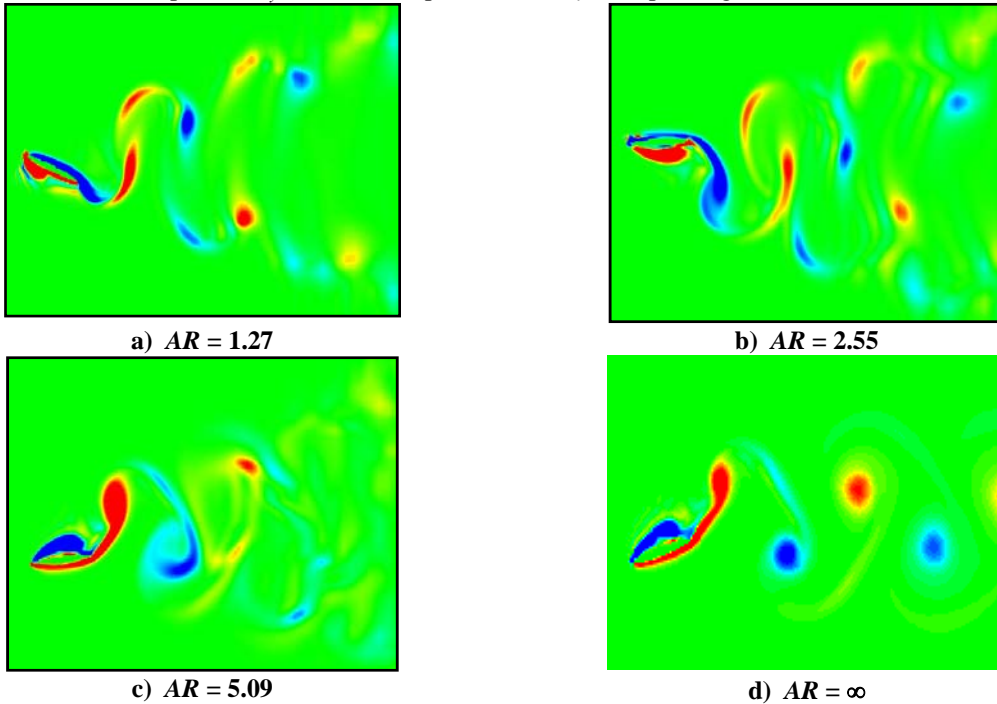


Figure 6. Center-plane spanwise vorticity contours for thrust-producing flapping foils. $St = 0.6$.

For any fixed aspect-ratio including the 2-D case, mean thrust coefficients monotonically increase with the increasing of Strouhal numbers. However, the propulsive efficiency in Figure 9b reaches to a peak value at a certain Strouhal number first, and then reduces after that point. The location of the peak is however different for different aspect-ratios. The larger the aspect-ratio, the larger the peak value and smaller the Strouhal number where the peak

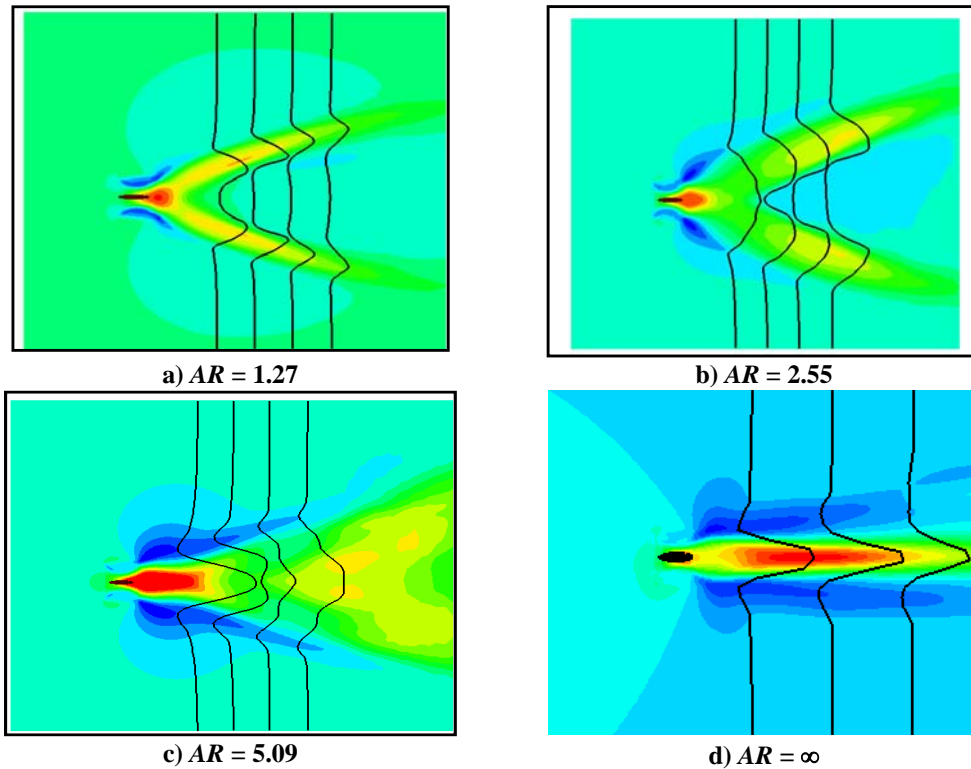


Figure 7. Center-plane time-averaged streamwise velocity contours. Black lines are the streamwise velocity profiles

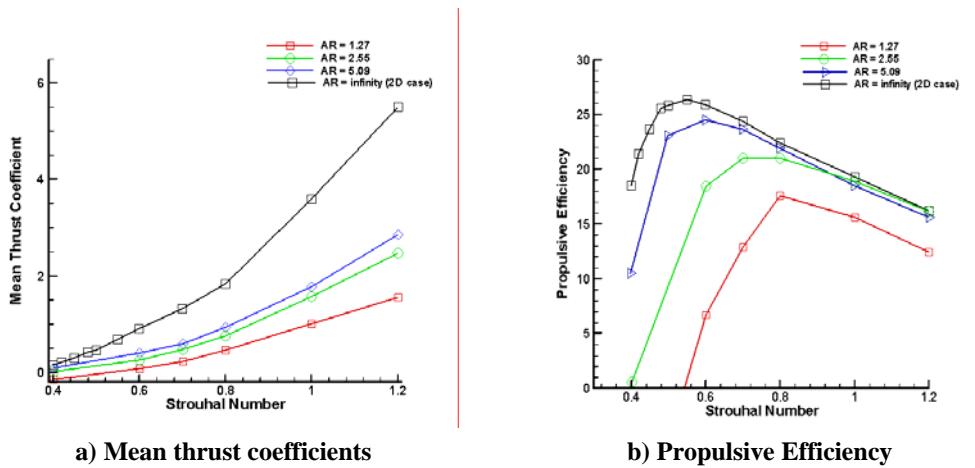


Figure 8. Comparisons of mean thrust coefficients and propulsive efficiency for different Strouhal numbers.

is found. For high enough aspect-ratio, all but the lowest aspect-ratio foils are found to reach similar values of efficiency.

In the next set of simulations, the Reynolds number is varied from 100 to 400 at a fixed aspect-ratio, $AR = 2.55$, and fixed Strouhal number, $St = 0.6$ to examine the Reynolds number effect on the wake structure and foil performance.

Figure 9 shows the differences of the wake structures for Reynolds number 100, 200, and 400 respectively, where all three cases are thrust-producing cases. The structure of the vortex structures in the downstream becomes more complicated with increasing of Reynolds number due to the appearing of more interconnections between those two sets of vortex rings. Moreover, the inclined angle of the vortex rings also changes wherein the vortex rings become more vertically aligns with increasing Reynolds number. This is expected to increase the thrust and this can be verified in Figure 10, which shows the comparison of the mean thrust coefficients and the propulsive efficiency for this study. The Reynolds number 400 case has almost twice larger thrust and propulsive efficiency compared to the Reynolds number 100 case. The variation of Reynolds number can therefore strongly affect the foil performance at least at these relatively low Reynolds numbers.

Change in the pitch-bias angle has a significant effect on the hydrodynamic forces produced by the flapping foil [12] and in the next set of simulations, we study the pitch-bias effects on the wake topology and the hydrodynamic performance of the flapping foils. The aspect-ratio, Strouhal number and Reynolds number are fixed at values of 2.55, 0.6 and 200 respectively and the pitch-bias angle, α_o , is varied from 0° to 30° .

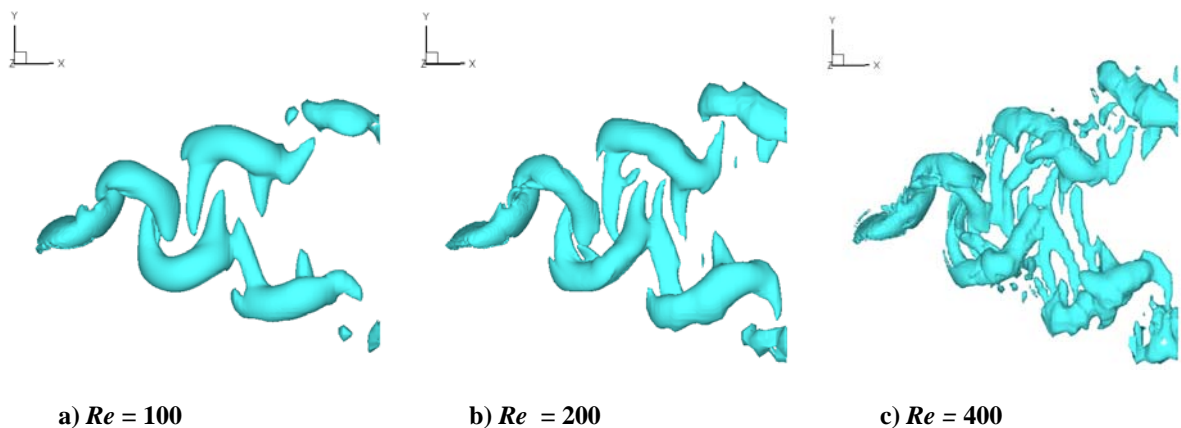


Figure 9. Side view of vortex topology plots for $AR = 2.55$ flapping foil at different Reynolds numbers.

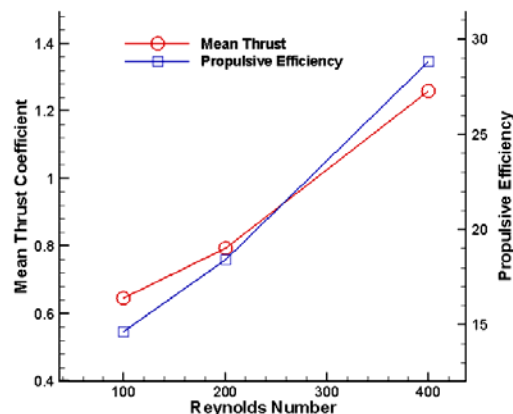


Figure 10. Comparisons of mean thrust coefficients and propulsive efficiency for different Reynolds numbers for $AR=2.55$ and $St=0.6$ flapping foil.

Figure 11 shows the 3-D wake structures of different pitch-bias angles. At pitch-bias angle of 0° , two sets of vortex rings with equal strength are formed. The jets formed by these two set of rings equally contribute to the thrust production of the flapping foil and zero lift force is expected. As seen in Figure 11b and Figure 11c, when pitch-bias angle increases, one of those two sets of vortex rings becomes weaker and the other one grows. These two unbalanced sets of vortex rings make different contributions to the thrust and lift force produced by the foil. Meanwhile the inclination angle of vortex rings also changes. As a result of this, thrust and lift force are modified significantly. The combined effect of the change in mean thrust and lift coefficients is shown in polar plot in Figure

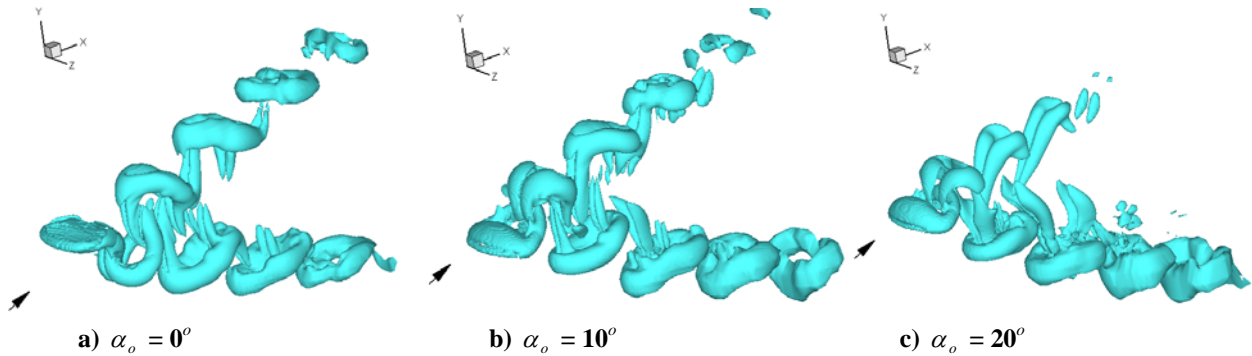


Figure 11. Side view of wake structures of flapping foils at different pitch-bias angles.

12. It can be seen that small changes in the pitch-bias angle can produce large changes in the mean lift. This suggests that the pitch-bias would be an effective control parameter for producing pitch-up force and rolling moment for rapid and precise maneuvering. The simulations also indicate that that for a bias angle greater than about 18° , the foil produces negative thrust. This is inline with the recent experiments of Triantafyllou et al. [12]

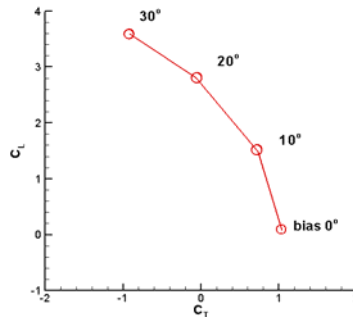


Figure 12. Mean thrust and lift coefficients for pitch-bias study

IV. Summary

An efficient finite-difference based solver for simulating flows with moving immersed boundaries on fixed Cartesian grids has been used to explore the wake structures and the hydrodynamic performance of finite aspect-ratio flapping foils. The simulations indicate that the wake topology of these relatively low aspect-ratio foils is significantly different from that observed for large and infinite aspect-ratio foils. Lower aspect-ratio foils are in general found to produce less thrust than high aspect-ratio foils and also have a lower propulsive efficiency. For the relatively low Reynolds numbers investigated in the current study, it is found that increase in Reynolds number can significantly improve the thrust performance of the flapping foil. Effect of pitch-bias on vortex topology and thrust performance has also been studied.

Acknowledgement

This work is supported under ONR Grants N00014-03-1-0458 and N00014-03-1-0897.

References

- ¹F. E. Fish, G. V. Lauder, R. Mittal, A. H. Techet, M. S. Triantafyllou, J. A. Walker, and P. W. Webb., "Conceptual Design for the Construction of a Biorobotic AUV Based on Biological Hydrodynamics," *Proceedings of 13th International Symposium on Unmanned Untethered Submersible Technology (UUST)*, Durham, New Hampshire, 2003.
- ²Tuncer, I. H. and Platzer, M. F., "Computational Study of Flapping Airfoil Aerodynamics," *AIAA Journal of Aircraft*, Vol. 37, No. 3, 2000, pp. 514, 520.
- ³Jones, K. D., Lai, J. C. S., Tuncer, I. H. and Platzer, M. F., "Computational and Experimental Investigation of Flapping-Foil Propulsion," *1st International Symposium on Aqua Bio-Mechanisms / International Seminar on Aqua Bio-Mechanisms*, Tokai University Pacific Center, Honolulu, Hawaii, 2000.
- ⁴Ramamurti, R., Sandberg, W. C., Löhner, R., Walker, J.A. and Westneat, M.W., "Fluid Dynamics of flapping aquatic flight in the bird wrasse: three-dimensional unsteady computations with fin deformation," *J. Exp. Biol*, Vol. 205, No. 19, 2002, pp. 2997, 3008.
- ⁵Koochesfahani, M. M., "Vortical Patterns in the Wake of an Oscillating Airfoil," *AIAA 87-0111, AIAA 25th Aerospace Sciences Meeting*, Reno, NV, 1987.
- ⁶Triantafyllou, G. S., Triantafyllou, M. S., and Grosenbaugh, M. A., "Optimal thrust development in oscillating foils with applications to fish propulsion," *J. Fluids Struct.*, Vol. 7, 1992, pp. 205, 224.
- ⁷Mittal, R., Akhtar, I., Bozkurtas, M., and Najjar, F. M., "Towards a Conceptual Model of a Bio-Robotic AUV: Pectoral Fin Hydrodynamics," *13th International Symposium on Unmanned Untethered Submersible Technology*, 2003.
- ⁸Ye, T., Mittal R., Udaykumar, H. S., and Shyy W., "An accurate Cartesian grid method for simulation of viscous incompressible flows with complex immersed boundaries," *J. Comput. Phys.*, Vol. 156, 1999, pp. 209, 240.
- ⁹Udaykumar, H. S., Mittal R., Rampunggoon, P., and Khanna, A., "A Sharp Interface Cartesian Grid Method for Simulating Flows with Complex Moving Boundaries," *J. Comput. Phys.*, Vol. 174, 2001, pp. 345, 380.
- ¹⁰Bozkurtas, M., H. Dong, R. Mittal, and F. Najjar, "Towards Numerical Simulation of Flapping Foils on Fixed Cartesian grids," *AIAA 2005-0081*, Reno, NV, 2005
- ¹¹Drucker, E., and Lauder G., "Experimental hydrodynamics of fish locomotion: functional insights from wake visualization," *Integ. and Comp. Biol.*, Vol. 42, 2002, pp. 243, 257.
- ¹²Triantafyllou, M. S., Hover, F.S. and Licht, S., "The Mechanics Of Force Production In Flapping Foils Under Steady-State And Transient Motion Conditions," MIT Department of Ocean Engineering, Testing Tank Facility Report 031903, 2003.
- ¹³Ramamurti, R., and Sandberg, W. C., "A Three-Dimensional Computational Study of the Aerodynamic Mechanisms of Insect Flight," *J. Exp. Biol*, Vol. 205, No. 10, 2002, pp. 1507, 1518.
- ¹⁴Liu, H., Ellington, C.P., Kawachi, K., van den Berg, C., and Willmott, A. P., "A Computational Fluid Dynamic Study of Hawkmoth Hovering," *J. Exp. Biol*, Vol. 201, No. 4, 1998, pp. 461, 477.
- ¹⁵Soria, J., and Cantwell, B. J., "Identification and Classification of Topological Structures in Free Shear Flows," Eddy Structure Identification in *Free Turbulent Shear Flows* edited by J. P. Bonnet and M. N. Glauser, 1993, pp 379-390.
- ¹⁶von Ellenrieder, K. D., Parker, K., and Soria, J., "Flow Structures Behind a Heaving and Pitching Finite-Span Wing," *Journal of Fluid Mechanics*, Vol. 490, 2003, pp. 129, 138.